Hardware Implementation of a Dynamic Mode Decomposition Algorithm for Feature Extraction of High-Impedance Faults

Javier Hernández-Alvídrez, *Member, IEEE*, Miguel Jiménez-Aparicio, *Member, IEEE*, Oscar S. Acosta, *Member, IEEE*, and Matthew J. Reno, *Senior Member, IEEE*
Electric Power Systems Research
Sandia National Laboratories
Albuquerque, NM
{jherna4, mjimene, osacost, mjreno}@sandia.gov

***Abstract*—Undetected high-impedance faults (HIF) in distribution systems pose a public safety risk in urban and rural areas, as they have the potential to cause electrical shock to humans or animals. Moreover, for cases where a toppled power line causes the HIF, the induced electric arc can ignite a wildfire if it comes into contact with dry vegetation in a forested area. For these reasons, industry professionals and researchers, particularly in the field of protective relaying, have worked for decades on developing viable and practical solutions to HIF detection. Over the last decade, most of these solutions have focused on improving the signal feature classification of HIF with the aid of artificial intelligence (AI) schemes. However, the exploration of new methodologies to identify the signal features of HIF has stalled. This paper presents a pragmatic and novel approach for implementing an online dynamic mode decomposition (DMD) algorithm for identifying HIF features. The algorithm was programmed into a commercial DSP board and operates in real time. It was tested using recorded signals from staged downed conductors as inputs. While continuously monitoring the real part of the lead eigenvalue calculated by the DMD routine, the algorithm revealed insightful signal features during the presence of HIF. Recommendations were provided, not only on the use of such features as HIF diagnostic elements, but also on best practices for implementing the DMD algorithm in an embedded device. This approach provides a practical solution to advance the state of the art in incorporating new analytical tools for the future generation of commercial protective relays.**

Keywords—high impedance faults, public safety, protective relay, dynamic mode decomposition, distribution systems, digital signal processing.

I. Introduction

To further modernize the power grid, novel, flexible protection schemes are needed to enhance the safety, security, and reliability of the designated protection zones. The schemes must address emerging protection challenges related to aging infrastructure, disaggregation of firm capacity, and contingencies for weather-related events. Furthermore, the rapid increase in electricity demand from AI data centers will require a different approach to protect the grid supplying them while maintaining the power system's resiliency. Failure to act promptly on these issues could significantly increase the likelihood of large, more frequent blackouts [1].

Among the most difficult anomalies to detect in power grids are high-impedance faults (HIF). This phenomenon occurs when a conductor in a power distribution system inadvertently comes into contact with a low-conductivity object. The high-impedance of such an object reduces the fault current's magnitude, preventing it from reaching the protective relay's overcurrent tripping threshold. An undetected HIF can pose significant public safety hazards by creating exposed electric arcs that may lead to electrocution. Moreover, such arcs could ignite severe wildfires and cause disastrous economic losses when they come into contact with dry vegetation in forested areas [1], [2].

Since the early 1970s, industry professionals and researchers have proposed several schemes and techniques to detect HIF by extracting signal features from faulted traces. Most of these techniques reflect the current state of the art of the analytical tools available at the time they were developed. A thorough and detailed account of the historical efforts to address the HIF issues is presented in [3], highlighting the early schemes that laid the analytical foundations based on frequency components (not the fundamental) and voltage sequences. By the 1990s, leading research entities in the field realized that a single scheme could not address all HIF variations. Thus, ad hoc algorithms based on HIF classification began to emerge [4]. The advent of affordable digital computers and significant improvements in computational power and memory size began to play a role in the emergence of simulation models outlining the dynamics of HIF [5], [6]. By the 2000s, advancements in embedded systems with digital signal processing (DSP) capabilities enabled protective relay manufacturers to begin incorporating digital solutions to monitor and detect HIF by implementing real-time algorithms [7], [8]. During the contemporary era (following the 2010s, as per [3]), the use of artificial intelligence (AI) has begun to increase [9]. Such methods have mainly been used to classify HIF signal features based on frequency analysis, voltage-sequence components, and mathematical morphology [10], [11], [12], [13]. The literature in this regard is vast and has a significant impact on fault location schemes; however, efforts to explore new analytical tools to identify HIF signal features have stalled [3].

The work presented in [14], [15], [16] follows a similar chronology (but in a shorter time span) to the one shown above by first identifying a readily available analytical tool, called dynamic mode decomposition (DMD), which can be used to extract HIF signal features that provide insightful information to machine learning (ML) algorithms for fault classification and fault location. Initially, DMD was used to identify high-frequency features in low-impedance faults, but the work presented in [17] demonstrates its applicability to HIF detection and classification. With the work mentioned above, which lays the theoretical foundations for using DMD to identify abnormal power-quality events, the next logical step is to implement a real-time online DMD algorithm, enabling its incorporation into a field-deployable prototype relay.

This paper presents a hardware implementation of a real-time DMD algorithm specifically tailored to analyze sets of three-phase signals to identify features that lead to HIF

979-8-3315-8138-1

detection and classification. To validate the proposed DMD implementation, recordings from a staged HIF were used to test the hardware in real-time.

II. Fundamentals of Dynamic Mode Decomposition

Essentially, DMD is a data-driven technique that constructs reduced linear models from complex, high-dimensional systems by extracting their dominant dynamical patterns [18]. This emerging technique, which originated in the field of fluid dynamics, has been recently applied to other fields, including robotics, neuroscience, and finance. One of the main advantages of DMD is that, as a purely data-driven method, it requires no derivation of the system's underlying dynamical equations. Furthermore, DMD is applicable to systems that are not strictly linear [18].

The first step in performing DMD is to collect the data and organize it into the appropriate matrices, as illustrated in Fig. 1, where the two main data matrices, X and Y (both of size n by k), are depicted. Each matrix is formed by collecting sets of instantaneous samples (vectors x_i and y_i) containing n measurements, and taken at equidistant time intervals, Δt (fixed sampling rate). The matrix X is formulated by stacking the first k samples (i.e., x_1 to x_k) within the rectangular dashed window shown in Fig. 1. The matrix Y, on the other hand, is formulated by stacking the last k samples of that very same window. From a different perspective, matrix Y is just matrix X, but one time step ahead. Thus, both matrices are almost identical, except for their first and last samples. At the moment, it may seem redundant to have two labels for one sample (i.e., $y_i = x_{i+1}$, with $1 \leq i \leq k\text{-}1$); however, this notation will come in handy when deriving and understanding the online DMD algorithm for three-phase systems, as shown in the next section.

The main objective of DMD is to find a linear operator A that advances matrix X into matrix Y. In other words, A becomes a matrix projector that best fits the approximation:

$$Y \approx A \cdot X \ . \tag{1}$$

Thus, finding A becomes an optimization problem constrained by the function:

$$\sum_{i=1}^{k} \|y_i - Ax_i\|^2 = \|Y - AX\|_F^2 \ , \tag{2}$$

where F refers to the Frobenius norm. The summation term in (2) provides the main mathematical insight into DMD, which is to minimize the sum of the Euclidean distances between each column vector in Y and each column vector in AX.

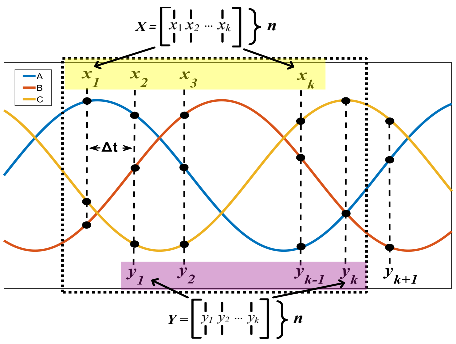

Fig. 1. Formulation of data matrices for the DMD algorithm.

Equations (1)-(2) represent a least squares problem; hence, the solution for the linear operator A is given by:

$$A = YX^+ \ , \tag{3}$$

where X^+ represents the Moore-Penrose pseudoinverse of X, which is given by:

$$X^+ = X^T(XX^T)^{-1} \ , \tag{4}$$

where X^T denotes the transpose of X. To develop intuition about the importance of the linear operator A, it is essential to go back to (1). Since A allows for the best fit projection of X onto Y by minimizing the Euclidean distance between the two matrices, this suggests that A and its corresponding eigenvalues possess insightful information about the dominant dynamical modes of the system under study [18]. For instance, if DMD is applied to a set of balanced three-phase electrical signals like the one shown in Fig. 1, it is expected that the dominant dynamical mode of A reveals the behavior of the fundamental frequency in the corresponding leading eigenvalue.

The calculation of A using (3) and (4) represents the standard DMD implementation [21] and is suitable for characterizing systems with slow dynamics [18]. This implementation requires full matrix operations, which utilize a substantial amount of computational resources. Every time a new sample is added to X and Y, the matrix operations must be repeated to update A. This DMD implementation is not feasible for systems with fast dynamics that require periodic and rapid monitoring, such as the power grid. Consequently, a modern extension to the theory of DMD is necessary to reduce the computational burden of calculating A. Such an extension is referred to as windowed online DMD. It focuses on updating A by utilizing only the new set of samples added, while preserving the analytical essence of the standard DMD. The following section focuses on the derivation and key mathematical details of this DMD extension.

III. Online Dynamic Mode Decomposition

Online DMD allows the update of the linear operator A in (1) without performing the full matrix multiplications in (3) and (4) that involve all the elements in X and Y. Instead, online DMD only uses the most recent and the very last samples within the sliding data window, as depicted in Fig. 2, where A_k denotes the linear operator A calculated up to sample k. Similarly, A_{k+1} corresponds to the updated linear operator once the new sample becomes available. The central premise underlying the formulation of the online DMD algorithm relies on the fact that, since only one sample is added, the updated matrix A_{k+1} must be somehow related to A_k [19].

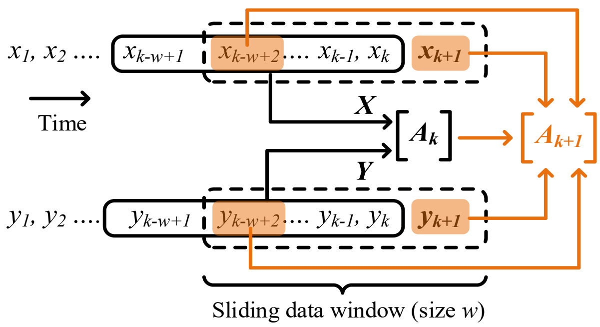

Fig. 2. Online DMD algorithm.

The starting point of the online DMD algorithm derivation is to substitute (4) into (3), which gives:

979-8-3315-8138-1

$$A_k = Y_k X_k^T (X X_k^T)^{-1} = M_k N_k \,, \quad (5)$$

$$M_k = Y_k X_k^T = \sum_{i=k-w+1}^{k} y_i x_i^T \,, \quad (6)$$

$$N_k = (X_k X_k^T)^{-1} = \left(\sum_{i=k-w+1}^{k} x_i x_i^T\right)^{-1}, \quad (7)$$

where the subindex k denotes the latest sample within the sliding data window of size w. As the new sample (denoted with index $k+1$) becomes accessible, (5) to (7) can be expressed as follows:

$$A_{k+1} = M_{k+1} N_{k+1} \,, \quad (8)$$

$$M_{k+1} = M_k - y_{k-w+1} x_{k-w+1}^T + y_{k+1} x_{k+1}^T \,, \quad (9)$$

$$N_{k+1}^{-1} = N_k^{-1} - x_{k-w+1} x_{k-w+1}^T + x_{k+1} x_{k+1}^T \,. \quad (10)$$

Equation (9) demonstrates the similarities between M_{k+1} and M_k. On the right side of (9), notice that M_k is modified by: i) subtracting the product of two terms involving only the last elements of the data window, and ii) adding the product of two terms involving only the last samples of the data window (see Fig. 2). The same can be said about (10). Finally, substituting (9) and the inverse of (10) into (8), renders:

$$A_{k+1} = A_k + (F - A_k G)(H^{-1} + G^T M_k G)^{-1} G^T M_k \,, \quad (11)$$

where the matrices F, G, and H are defined as follows:

$$F = [y_{k-w+1} \quad y_{k+1}] \,, \quad (12)$$

$$G = [x_{k-w+1} \quad x_{k+1}] \,, \quad (13)$$

$$H = \begin{bmatrix} -1 & 0 \\ 0 & 1 \end{bmatrix} . \quad (14)$$

The derivation of (11) is not a straightforward task. It requires the use of advanced linear algebra identities, such as the Sherman-Morrison identity [20], which helps simplify the inversion of matrix N_k in (10). The reader is encouraged to study the complete and detailed derivation of (11) in the pioneering work on online DMD presented in [19].

IV. Implementation of DMD for HIF Detection

The proposed hardware implementation utilizes a readily available embedded system with DSP capabilities from Texas Instruments, specifically the TI TMS320F28388 from the C2000 family. It is a dual-core microcontroller operating at a clock speed of 200 MHz. The main algorithm (firmware) is illustrated in Fig. 3 and comprises three primary routines: the initial DMD matrix generation routine, the online DMD routine, and the eigenvalue computation routine. As an aside, from hereon, the term 'sample' will refer to a vector containing the three simultaneous measurements corresponding to phases *abc* of an electrical system.

A. Initial DMD Matrix Generation Routine

This routine computes A_0, which is the initial matrix that serves as a baseline for further iterations of this linear operator. To create A_0, this routine relies on the DSP's embedded analog-to-digital converters (ADC) to collect the initial w samples at a programmable sampling frequency, f_s. With the collected samples in memory, the routine calculates A_0 using (3) and (4), which is the standard DMD approach. This calculation is performed only once, at the very beginning of the DMD algorithm.

B. Online DMD Matrix Update Routine

This routine computes A_{k+1} using (8), with the aid of (9) and (10) as intermediate steps. It utilizes a circular buffer to form the sliding data window of size w, as shown in Fig. 2. The first task is to acquire and store the new sample. Following this, the routine adjusts the data window by sliding it one step forward and maintaining its size constant. Moreover, both the latest and the last samples of the data window are used in (9) and (10), which are required to update A_{k+1} using (8).

C. Eigenvalue computation routine

The lead eigenvalue of the updated A_{k+1} matrix provides direct and insightful information about the instantaneous dynamics of the system under study. If such a system is a balanced set of three-phase signals, the imaginary part of the lead eigenvalue will reveal the fundamental frequency, whereas the real part will remain constant. However, if a disturbance in power quality is present, such as a HIF, the real part of the lead eigenvalue reveals unique dynamics whose signal features can be used to detect and correlate with the presence of a HIF.

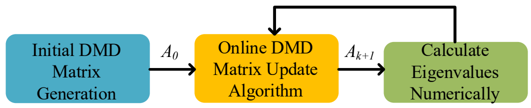

Fig. 3. Main routines of the DMD algorithm implementation in the DSP.

The implemented routine is an iteration-based numerical scheme that reveals the eigenvalues of A_{k+1} by utilizing the QR factorization as its primary task. The flow diagram in Fig. 4 illustrates the central tasks of the routine. It starts by passing A_{k+1} to a local variable array called T_{i-1}, and also by setting the maximum number of iterations, m. Then, it performs the Q_iR_i factorization on T_{i-1} followed by the formulation of a new T_i, which is the reverse multiplication of the previously computed QR factors. This formulation operates as a similarity transformation, which changes the values of T in every iteration, but preserves the eigenvalues of the initial matrix A_{k+1} at all times [21]. If sufficient iterations are performed, T will converge to an upper triangular matrix, whose diagonal elements reveal the eigenvalues. To improve the rate of convergence and minimize the risk of floating-point instability (thus, improving the reliability of the whole algorithm), the QR factorization routine uses the Householder reflector technique, which provides a more reliable and safe mechanism for finding the QR factors than the common Gram-Schmidt technique [21].

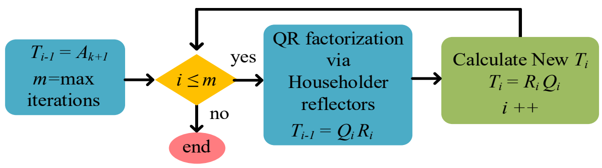

Fig. 4. Main tasks of the eigenvalues computation routine.

V. HIF Testing Setup

To validate the online DMD algorithm, the testing setup shown in the left picture of Fig. 5 was implemented. The main component of the testing setup is the in-house designed fault playback recorder capable of replicating a set of low-voltage three-phase signals under abnormal utility events, such as HIF. The playback device was programmed to reproduce HIF current traces (at an output frequency of 400 kHz), based on the staged HIFs reported in [4], whose voltage-current (VI) characteristics are depicted in the right plot of Fig. 5. The oscillographs in Fig. 6 show the voltage and current behavior

979-8-3315-8138-1

when the above VI characteristics are programmed in the fault playback recorder.

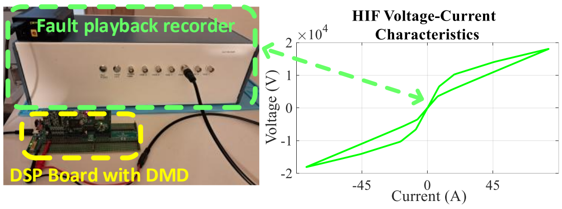

Fig. 5. Testing setup used to validate the DMD algorithm to detect HIF.

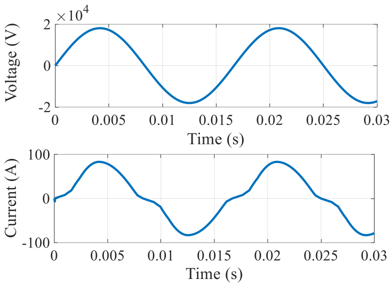

Fig. 6. Oscillography provided by the fault playback recorder.

VI. Experimental Results

The algorithm was validated using the testing setup mentioned above. One of the phases of the set of three-phase currents was programmed to display the VI characteristics in Fig. 5, with a trace similar to the one shown at the bottom of Fig. 6. To identify unique HIF signal features, the real component of the leading eigenvalue was monitored and recorded during and after a HIF occurrence. As reported in [16], [17], the monitoring of the real component of the eigenvalue provides insightful signal features that aid in discriminating HIF. However, these references used the standard DMD approach to validate the usefulness of the algorithm, but a real-time approach was not attempted.

A. *Accuracy vs sampling frequency*

The ADCs' sampling frequency is limited by the number of iterations the algorithm uses to compute the eigenvalues. However, a minimum number of iterations is required to ensure that the calculated lead eigenvalue is accurate. For this reason, it is essential to find a balance between these two parameters to maximize sampling speed without downplaying accuracy. Using offline simulations, it was determined that after 12 iterations, the calculated eigenvalue matched the theoretical value. The traces in Fig. 7 were obtained using the above testing setup with the DMD algorithm running at 20 kHz. They show the dynamics of the real component of the lead eigenvalue before and after a HIF. Each trace corresponds to a different number of iterations used to calculate the real component. From the traces, notice how the use of only 1 iteration (blue trace) does not converge to the actual value. However, note that after 3 iterations, the difference with respect to the 12-iteration trace reduces significantly. Table I summarizes the computational burden (in microseconds) incurred by the DSP for each number of iterations used, as well as the maximum sampling frequency limit imposed by such burden. To perform the time measurements of the computational burdens, an output pin of the DSP was set at the beginning of the eigenvalue calculation routine as the initial marker. Then, at the end of the routine, the pin was cleared and the pulse width was measured. From the traces in Fig. 7 and the data in Table I, it can be observed that using 6 iterations provides a high degree of accuracy without significantly compromising the sampling rate. Based on this observation, the remaining experiments will be conducted using 6 iterations.

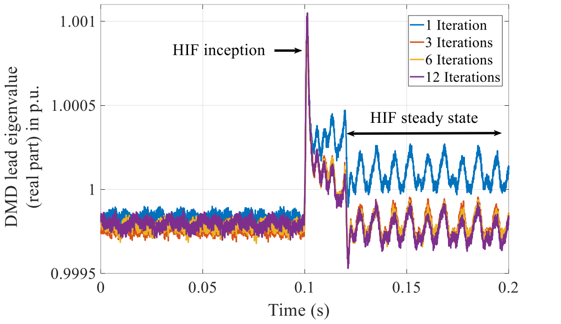

Fig. 7. Traces showing the real component of the lead eigenvalue with the number of iterations as a parameter.

TABLE I. DSP'S COMPUTATIONAL BURDEN COMPARISON.

Number of iterations	Computational burden (μs)	Maximum allowable sampling rate (kHz)
1	8.2	122
3	12.2	82
6	18.2	55
12	30.0	33.3

B. *Sampling rate impact for a constant window size.*

The traces in Fig. 8 show the dynamics of the real component of the lead eigenvalue at different sampling frequencies. At the same time, the sliding data window was maintained at an equivalent length of exactly one fundamental AC cycle. Upon HIF inception, the three traces exhibit an initial overshoot, followed by similar oscillations with higher amplitudes as the sampling frequency decreases. The initial overshoot is also higher as the sampling frequency decreases, and could serve as a triggering action for HIF detection. In contrast, the subsequent oscillations could be utilized as discriminating features for HIF classification using advanced diagnostic techniques, such as shapelets. Also, notice that after the oscillations are damped, no discernible features remain, which hinders the detection of a sustained HIF. Finally, if data memory is limited, it is recommended to use the lowest sampling rate, as this mode requires fewer memory elements to implement the circular buffer representing the data window.

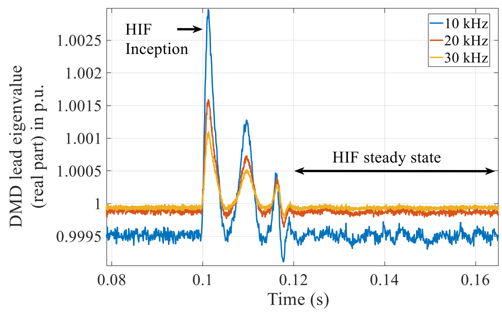

Fig. 8. DMD eigenvalue traces at different sampling frequencies.

C. *Window size impact for a constant sampling frequency.*

The traces in Fig. 9 illustrate the dynamics of the lead eigenvalue's real component as the data window size is adjusted, while maintaining a constant sampling frequency of 20 kHz. The plot at the top shows the traces corresponding to window sizes of one and two fundamental AC cycles. Notice

979-8-3315-8138-1

the presence of the initial oscillations that can be used as the initial signal-related symptoms of the presence of a HIF. Nevertheless, if the HIF is sustained, these data window sizes do not reveal insightful features indicating the presence of HIF. The plot at the bottom of Fig. 9 shows the traces for window sizes of 1.2 and 1.7 cycles (fractional cycle window). From this plot, notice also the initial spike followed by a transient with non-noticeable oscillations; however, during the steady-state interval, the eigenvalue dynamics reveal signal features that can aid in the diagnosis and classification of a sustained HIF [17]. These captured HIF steady-state dynamics are due to the fact that the fractional windows allow the identification of interharmonic signal features [18].

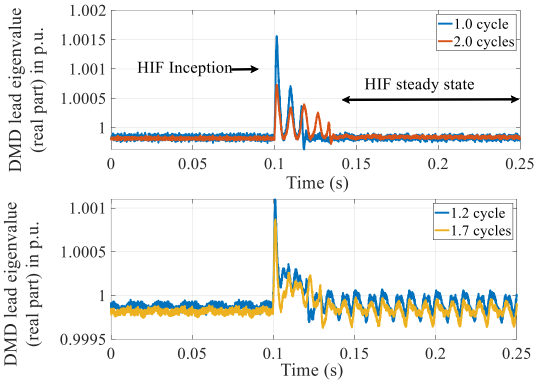

Fig. 9. DMD Eigenvalue traces using different data window sizes.

VII. Conclusions

A real-time hardware implementation of a DMD algorithm to identify signal features of a HIF is presented. On a sample-by-sample basis, the algorithm's routine updates the main DMD matrix and obtains its leading eigenvalue. To improve the numerical stability and accuracy of the algorithm, the eigenvalue numerical computation routine employs the Householder reflector scheme, which also facilitates the acceleration of the conversion rate. The use of 6 iterations on such eigenvalue routine provided a good tradeoff between accuracy and maximum sampling frequency. The algorithm was tested using a set of staged three-phase currents undergoing a HIF, and the real component of the lead eigenvalue was recorded and analyzed. The tests included variations in sampling frequency and data window size. The main findings from the tests at different sampling frequencies indicated an impact on the amplitudes of the initial transient spikes at HIF inception. The data window size tests revealed that if the size of the window is equivalent to an integer multiple of the fundamental cycle, the eigenvalue dynamics show initial oscillations that can aid in the identification of HIF; however, after the oscillations dampen, no discernible features are observed. If the data window's size is not a multiple of the fundamental cycle, the initial oscillations are not noticeable, but the steady state dynamics reveal useful signal features that can help to diagnose the presence of a sustained HIF.

Acknowledgment

This article has been authored by an employee of National Technology & Engineering Solutions of Sandia, LLC under Contract No. DE-NA0003525 with the U.S. Department of Energy (DOE). The employee owns all right, title and interest in and to the article and is solely responsible for its contents. The United States Government retains and the publisher, by accepting the article for publication, acknowledges that the United States Government retains a non-exclusive, paid-up, irrevocable, world-wide license to publish or reproduce the published form of this article or allow others to do so, for United States Government purposes. The DOE will provide public access to these results of federally sponsored research in accordance with the DOE Public Access Plan https://www.energy.gov/downloads/doe-public-access-plan.

References

[1] "Gridware - PG&E Battles High Impedance Faults." Accessed: Oct. 23, 2025. [Online]. Available: https://www.gridware.io/case-studies/pgae-battles-high-impedance-faults

[2] A. Rahiminejad, D. Hou, N. Nakamura, and M. Bundhoo, "Fire Mitigation for Distribution Achieve Quick Progress With Advanced Technology Solutions," 2021.

[3] D. P. S. Gomes and C. Ozansoy, "High-impedance faults in power distribution systems: A narrative of the field's developments," *ISA Trans*, vol. 118, pp. 15–34, Dec. 2021, doi: 10.1016/J.ISATRA.2021.

[4] C. L. Huang, H. Y. Chu, and M. T. Chen, "Algorithm comparison for high impedance fault detection based on staged fault test," *IEEE Transactions on Power Delivery*, vol. 3, no. 4, pp. 1427–1435, 1988.

[5] R. E. Lee and M. T. Bishop, "A Comparison of Measured High Impedance Fault Data to Digital Computer Modeling Results," *IEEE Power Engineering Review*, vol. PER-5, no. 10, pp. 35–36, 1985.

[6] R. E. Lee and R. H. Osborn, "A microcomputer-based data acquisition system for high impedance fault analysis," *IEEE Transactions on Power Apparatus and Systems*, vol. PAS-104, no. 10, 1985.

[7] D. Hou, "Detection of High-Impedance Faults in Power Distribution Systems," in *33rd Annual Western Protective Relay Conference*, Clemson, Oct. 2006.

[8] Schweitzer Engineering Laboratories, "Arc Sense ™ Technology (AST)." Accessed: Oct. 25, 2025. [Online]. Available: https://cdn.selinc.com/assets/Literature/Product%20Literature/Flyers/Arc-Sense_PF00160.pdf?v=20161031-073656

[9] B. Hao, "AI in arcing-HIF detection: A brief review," *IET Smart Grid*, vol. 3, no. 4, pp. 535–544, Aug. 2020.

[10] J. V. De Souza, G. N. Lopes, J. C. M. Vieira, and E. N. Asada, "High Impedance Fault Detection in Distribution Systems: An Approach Based on Fourier Transform and Artificial Neural Networks," *2020 Workshop on Communication Networks and Power Systems.*

[11] B. Hao, L. Yuxin, L. Jieyi, L. Hongwen, L. Yipeng, and L. Ruigui, "High impedance fault detection device based on edge artificial intelligence," *Energy Reports*, vol. 9, pp. 546–550, Oct. 2023.

[12] F. Wilches-Bernal, M. Jimenez-Aparicio, and M. J. Reno, "An Algorithm for Fast Fault Location and Classification Based on Mathematical Morphology and Machine Learning," in *2022 IEEE Power and Energy Society Innovative Smart Grid Technologies Conference, ISGT 2022*.

[13] M. J. Aparicio, M. J. Reno, P. Barba, and A. Bidram, "Multi-resolution Analysis Algorithm for Fast Fault Classification and Location in Distribution Systems," in *2021 9th IEEE International Conference on Smart Energy Grid Engineering, SEGE 2021*, Institute of Electrical and Electronics Engineers Inc., Aug. 2021, pp. 134–140

[14] F. Wilches-Bernal, M. J. Reno, and J. Hernandez-Alvidrez, "A Dynamic Mode Decomposition Scheme to Analyze Power Quality Events," *IEEE Access*, vol. 9, pp. 70775–70788, 2021.

[15] F. Wilches-Bernal, M. Jimenez-Aparicio, and M. J. Reno, "A Machine Learning-based Method using the Dynamic Mode Decomposition for Fault Location and Classification," in *Twelfth Conference on Innovative Smart Grid Technologies (ISGT)*, 2021.

[16] F. Wilches-Bernal, M. J. Reno, and J. Hernández-Alvídrez, "Dynamic mode decomposition systems and methods to detect power quality events," 12,366,598, Jul. 22, 2025

[17] O. S. Acosta, M. Jimenez-Aparicio, J. Hernández-Alvídrez, and M. J. Reno, "A Novel High-Impedance Fault Detection Technique using Dynamic Mode Decomposition and Shapelets," Accepted for presentation, T&D Conference Chicago, Jul. 2026.

[18] S. L. Brunton and J. Nathan. Kutz, *Data-driven science and engineering : machine learning, dynamical systems, and control*. Cambridge University Press, 2022.

[19] H. Zhang, C. W. Rowley, E. A. Deem, and L. N. Cattafesta, "Online dynamic mode decomposition for time-varying systems," *SIAM J Appl Dyn Syst*, vol. 18, no. 3, pp. 1586–1609, Jul. 2017.

[20] J. W. Demmel, *Applied Numerical Linear Algebra*. Society for Industrial and Applied Mathematics, 1997.

[21] G. H. Golub and C. F. Van Loan, *Matrix Computations*. The Johns Hopkins University Press, 2013.

979-8-3315-8138-1